Performance evaluation of pre-stressed high-strength concrete pipe piles produced with steel slag powder and ground quartz sand as composite supplementary cementitious materials

Yang, Xinkui; Tu, Botao; Wu, Shaopeng; Xu, Shi; Song, Yu; Chen, Dongyu; Yang, Chao

DOI
10.1016/j.conbuildmat.2025.141451

Publication date
2025

Document Version
Final published version

Published in
Construction and Building Materials

Construction and Building Materials 478 (2025) 141451

Contents lists available at ScienceDirect

Construction and Building Materials

journal homepage: www.elsevier.com/locate/conbuildmat

Performance evaluation of pre-stressed high-strength concrete pipe piles produced with steel slag powder and ground quartz sand as composite supplementary cementitious materials

Xinkui Yang [a], Botao Tu [b], Shaopeng Wu [a,*], Shi Xu [c,d,**], Yu Song [a], Dongyu Chen [a], Chao Yang [e]

[a] State Key Laboratory of Silicate Materials for Architectures, Wuhan University of Technology, Wuhan 430070
[b] Guangdong Hongye Building Materials Technology Co., Ltd, Yunfu, Guangdong 527121, China
[c] School of Civil Engineering and Architecture, Wuhan University of Technology, Luoshi Road 122, Wuhan 430070, China
[d] Faculty of Civil Engineering and Geosciences, Delft University of Technology, Stevinweg 1, Delft 2628 CN, the Netherlands
[e] School of Civil Engineering, Architecture and Environment, Hubei University of Technology, Wuhan 430068, China

ARTICLE INFO

Keywords:
Pre-stressed high-strength concrete pipe pile
Steel slag powder
Ground quartz sand
Supplementary cementitious materials
Microstructure
Pore structure
Compressive strength

ABSTRACT

Utilizing industrial solid waste as supplementary cementitious materials (SCMs) in the production of pre-stressed high-strength concrete (PHC) pipe piles can reduce the consumption of cement, thereby promoting the sustainable development of the pipe pile industry. This study focused on optimizing the use of composite SCMs including ground quartz sand (GQS) and steel slag powder (SSP) to enhance the mechanical properties and durability of PHC pipe pile concrete. The effects of GQS and SSP on the reaction products, microstructure, pore structure, mechanical properties and durability of PHC pipe pile concrete were investigated. Experimental results showed that due to the filling effect and pozzolanic effect of GQS and SSP, composite SCMs not only improves the microstructure of the interfacial transition zone between paste and aggregates in PHC pipe pile concrete, but also reduces the porosity of concrete and improves its pore structure, thereby enhancing the compressive strength and durability of concrete. When the GQS content is 20 % and the SSP content is 10 %, compared to the control group with 100 % cement, the concrete's porosity decreased by 19.3 %, the chloride ion diffusion coefficient decreased by 47.1 %, and the compressive strength increased by 3.4 %. The findings of this study provide a scientific basis for the resource utilization of steel slag and offer theoretical support for the low-carbon and sustainable development of PHC pipe pile industry.

1. Introduction

Pre-stressed high-strength concrete (PHC) pipe piles, known for their excellent load-bearing capacity and suitability for various complex geological conditions, have emerged as a key structural material of foundation engineering in China [1–3]. as shown in Fig. 1, a large number of PHC pipe piles are produced annually in China to meet the growing demand in foundation engineering. The manufacturing process of PHC pipe piles typically involves steps such as concrete casting, pre-stressed tension, centrifugal molding, steam curing, and autoclave curing [4,5]. High-performance cementitious materials are the key to ensuring their mechanical properties and durability, but there are also problems such as high carbon emissions and cost [6,7]. The cement industry is the third-largest source of carbon emissions worldwide [8,9]. In recent years, China's increasing focus on sustainable development has driven innovation in the construction industry to reduce carbon emissions [10–13]. In this context, the production of PHC pipe piles urgently requires low-carbon and high-performance cement alternatives to mitigate carbon emissions and costs during the production process.

Supplementary cementitious materials (SCMs) are widely used as partial substitutes for cement to improve concrete's properties, such as workability, strength, and durability [14–16]. SCMs typically consist of industrial by-products and solid waste, because they are expected to promote the sustainable development of the construction industry while

* Corresponding author.
** Corresponding author at: School of Civil Engineering and Architecture, Wuhan University of Technology, Luoshi Road 122, Wuhan 430070, China.
E-mail addresses: wusp@whut.edu.cn (S. Wu), xushi@whut.edu.cn (S. Xu).

https://doi.org/10.1016/j.conbuildmat.2025.141451
Received 18 February 2025; Received in revised form 29 March 2025; Accepted 21 April 2025
Available online 23 April 2025

improving the performance of concrete [17–23]. Liu et al. [24] used fly ash (FA) as SCMs and investigated the effects of FA on the drying shrinkage and creep strain of concrete. The results indicated that when the FA content was 10 %, the drying shrinkage of concrete was minimized, whereas the lowest creep strain of concrete occurred at the FA content of 20 %. Shen et al. [25] employed granulated blast furnace slag (GBFS) as SCMs and studied its effect on the early-age cracking resistance of concrete. They found that GBFS inhibited the early-age shrinkage cracking of concrete. When 20 % of the cement was replaced with GBFS, the concrete's shrinkage strain at 28d was reduced by 11.1 %.

In addition to using a single type of solid waste as SCMs, recent studies have also explored the use of different types of solid waste as composite SCMs [15,26]. Composite SCMs typically involves the mixing of two or more solid waste to form composite materials with synergistic effects [27]. Bheel et al. [28] used coconut shell ash, metakaolin and calcined clay as composite SCMs to produce concrete. The results showed that when 10 % of the cement was replaced with composite SCMs, the tensile, flexural, and compressive strengths of the concrete increased by 9.62 %, 8.27 %, and 10.71 %, respectively. Liu et al. [29] used kaolin and limestone as composite SCMs and studied their effects on the mechanical and durability properties of concrete. The results indicated that the composite SCMs reduced the early-age compressive strength of concrete but significantly enhanced its resistance to chloride ion penetration and inhibited its volume expansion.

At present, ground quartz sand (GQS) has been widely used as SCMs to produce PHC pipe piles due to its stable supply in the market and relatively low price [30–32]. Yang et al. [33] used GQS as SCMs to produce PHC pipe pile concrete and investigated its mechanical properties. They found that with 30 % GQS content, the concrete's 28d compressive strength exceeded 90 MPa. Zhang et al. [5] replaced 30 % of cement with GQS to prepare PHC pipe pile concrete and investigated its mechanical properties and microstructure. They found that SiO_2 within GQS interacted with $Ca(OH)_2$, resulting in the formation of tobermorite, thereby increasing the concrete's compactness and mechanical strength. However, as a natural mineral resource, the use of GQS to produce PHC pipe piles does not fully meet the goal of low-carbon production and sustainable development. Therefore, further exploring other low-carbon and sustainable solid waste-based SCMs is crucial for pipe pile industry.

Therefore, in recent years, utilizing industrial solid wastes as SCMs in the manufacturing of PHC pipe piles has become the focus of research [32,34]. This approach helps reduce the production costs and carbon emissions of PHC pipe piles while promoting the resource recovery of industrial solid waste, thereby alleviating environmental burdens. Zhou et al. [6] used anhydrite and ground granular blast furnace slag (GGBFS) to produce PHC pipe pile concrete and analyzed its hydration process and microstructure. They found that the addition of GGBFS provided more amorphous reactive phases for the cementitious system, and the SO_4^{2-} in anhydrite will promote the early hydration reaction, thereby enhancing the compressive strength of concrete. Hu et al. [35] used fly ash (FA) as SCMs to prepare PHC mortar and examined the impact of FA on its porosity and durability. They found that incorporating FA reduced the porosity of PHC mortar, increased the content of gel pores, and thus enhanced its sulfate resistance.

Steel slag is a byproduct produced by the steel manufacturing sector [36–38]. In 2023, China's steel slag production was approximately 150 million tons, but its utilization rate was under 40 % [39,40]. Unused steel slag is often stored in open piles, leading to the waste of valuable land resources and posing a risk of heavy metal contamination [41,42]. The exposed steel slag can leach harmful substances into the surrounding environment, threatening soil and water quality and potentially impacting local ecosystems and human health [43,44]. Therefore, the utilization of steel slag is crucial to minimizing these environmental risks.

Steel slag has a mineral composition similar to cement, which gives it potential cementitious activity [45–47]. However, steel slag contains f-CaO and MgO, which pose a risk of volumetric expansion when it is used as cementitious material, but after aging treatment, the f-CaO in steel slag reacts and stabilizes, reducing its potential for expansion [48,49]. As a result, when the content of these two substances is within the acceptable limits, steel slag powder (SSP) can be safely used as SCMs to produce concrete. Zhuang et al. [50] used SSP and ultrafine blast furnace slag as composite SCMs to produce concrete, and studied the effects of SSP on concrete's strength, workability and autogenous shrinkage. The results show that SSP can reduce the heat release and the value of the temperature rise during the hydration process, thereby reducing the autogenous shrinkage of concrete and increasing its compressive strength. Luo et al. [51] used SSP as SCMs in mass concrete and found that the filling effect and delayed hydration of SSP could reduce the porosity of the concrete, as well as improve its setting time, fluidity and mechanical strength. Li et al. [52] replaced 30 % of cement with SSP to prepare paste and investigated the hydration products and microstructure of the composite binder under high-temperature steam conditions. The results indicated that high-temperature steam curing could shorten the hydration induction period of SSP and enhance paste's early strength. Moreover, its secondary hydration could further fill and refine the pores of paste, improving its long-term strength and durability. Considering that PHC pipe piles will also undergo high-temperature steam curing during production, the use of SSP as SCM is expected to improve the early strength and durability of PHC pipe piles.

However, due to the complex composition and relatively low reactivity of SSP, the study on its application in PHC pipe piles remains limited. In particular, compared to other commonly used SCMs, the reactive activity, reaction rate, and reaction products of SSP under autoclave curing conditions are uncertain, which poses challenges to the performance stability of PHC pipe piles produced by using SSP as SCMs. Therefore, how to enhance the applicability of SSP as SCMs in the production of PHC pipe piles through appropriate material mixing design remains one of the key challenges that requiring resolution.

This study aims to explore the feasibility of using SSP and GQS as

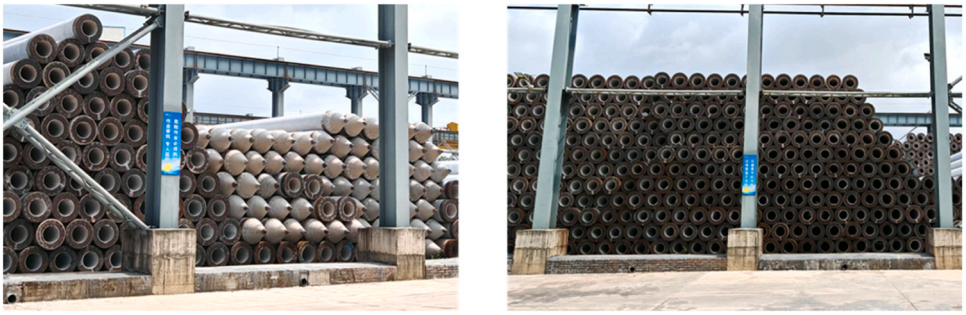

Fig. 1. PHC pipe piles piled up in the factory.

composite SCMs to produce PHC pipe pile concrete. The mechanical properties and durability of PHC pipe pile concrete were investigated through compressive strength test and rapid chloride ion migration (RCM) test. The phase assemblage, chemical functional groups and reaction products of PHC pipe pile concrete were evaluated using X-ray diffraction (XRD), Fourier transform infrared spectroscopy (FTIR) and thermogravimetric analysis (TGA). The microstructure and pore structure of PHC pipe pile concrete were investigated by scanning electron microscopy (SEM) and low field nuclear magnetic resonance (LF NMR). The research results can not only reveal the strength formation mechanism of PHC pipe piles produced by using GQS and SSP as SCMs, but also provide scientific basis for further realizing the resource utilization of SS, and provide theoretical support for the low-carbon and sustainable production of PHC pipe piles.

2. Materials and methods

2.1. Raw materials and mix proportions

In this study, SSP was sourced from Baowu Iron and Steel Group Co., Ltd., Wuhan, China, while GQS and P.O 42.5 Ordinary Portland Cement (OPC) were obtained from Hongyun Cement Co., Ltd., Guangdong, China. Table 1 displays the physical properties of OPC. The oxide compositions of SSP and GQS are summarized in Table 2, and the particle size and mineral composition of SSP and GQS are displayed in Fig. 2. It can be observed that SSP mainly consists of Fe_2O_3, CaO and SiO_2, while GQS mainly consists of SiO_2 and Al_2O_3. The XRD results indicate that the main mineral phase of GQS is quartz, while the main mineral phase of SSP includes mullite, quartz, CaO, C_3A, C_3S, C_2S, FeO and RO phase. The RO phase denotes the solidified metallic oxide solution resulting from slag's cooling in steel manufacture, its main components are FeO, MnO and MgO. Fig. 2(b) reveals that the average particle size of SSP and GQS are 48.31 μm and 17.01 μm, respectively. River sand, particle size < 1 mm, was chosen as the fine aggregate; its fineness modulus was 2.81 and the apparent density was 1549 kg/m^3. Graded gravel, particle size 5–25 mm, comprised the coarse aggregate. The polycarboxylate superplasticizer used in this study can reduce water dosage by 25 %.

Due to the presence of f-CaO and MgO in steel slag, these compounds can undergo hydration over time, leading to the formation of expansive products that may affect the volume stability of the concrete. Therefore, according to the Chinese standard GB/T 20491–2017 (Steel slag powder used for cement and concrete) [53], the stability of SSP used in this paper was evaluated by measuring the content of f-CaO and MgO in SSP. Specifically, the content of f-CaO was measured following the Chinese standard YB/T 4328–2012 (Method for the determination of free calcium oxide in steel slag) [54], while the MgO content was determined from the XRF results of the SSP. The results are presented in Table 3. It can be seen that the f-CaO and MgO contents of the SSP used in this study meet the standard requirements, indicating that its use as supplementary cementitious materials in concrete will not adversely affect the volume stability of the concrete.

Table 4 shows the detailed mixing proportion of concrete and paste specimens. For concrete specimens, the content of binder was fixed at 420 kg/m^3. According to the Chinese standard GB/T 51003–2014 [55], when using SSP as supplementary cementitious materials to produce concrete, its maximum content should not exceed 30 % of cement. At the same time, considering that an excessive amount of SCMs may reduce the concrete's mechanical properties, in this study, the SCMs content was fixed at 30 % of the total weight of binder. Furthermore, the proportions of GQS and SSP within the SCMs were adjusted to 3:0, 2:1, 1:2, and 0:3, respectively. To eliminate the influence of aggregate, paste specimens were prepared for microscopic test, in which the weight ratios of OPC, GQS, SSP, water and polycarboxylate superplasticizer are the same as those of concrete specimens. In addition, preparing mortar specimens to assess the cementitious activity of each group of SCMs, and the mix proportion is displayed in Table 5, where the weight ratios of OPC, GQS and SSP are the same as those in Table 4. The experimental research program of this study was shown in Fig. 3. The raw material preparation, mixing, curing and testing procedure in this study were shown in Fig. 4.

Table 1
Physical properties of OPC.

Physical properties		Measured values
Specific surface area (kg/m^3)		374
Normal consistency (%)		28
Setting time (min)	Initial set	198
	Final set	287
28d compressive strength (MPa)		42.7
28d flexural strength (MPa)		6.9

2.2. Preparation and curing regimes of specimens

For concrete specimens, OPC, GQS and SSP were initially dry-mixed for 1 min, followed by the addition of polycarboxylate superplasticizer and water, then wet-mixed for 2 min. Finally, fine aggregate and coarse aggregate were added to the mixer and mixed for an additional 3 min, and then cast into molds with a size of 100 mm × 100 mm × 100 mm. The concrete specimens' curing regimes are displayed in Fig. 5. The concrete with the mold was placed in a steam curing pool. The temperature was raised to 85 °C within 1.5 h, and the constant temperature was maintained for 4 h, and subsequently allowed to cool to room temperature for 1.5 h. After steam curing, the concrete specimens were taken out from the mold and placed in an autoclave. The pressure and temperature were increased to 1 MPa and 175 °C in 1.5 h and then kept for 6 h. The concrete specimens were taken out after cooling for 1.5 h. For paste specimens, OPC, GQS, SSP, water and polycarboxylate superplasticizer were mixed evenly in a mixer and then cast into 40 mm × 40 mm × 40 mm molds. and its curing regimes are the same as that of the concrete specimens. For mortar specimens, OPC, GQS, SSP, standard sand and water were mixed evenly in a mixer and then cast into 40 mm × 40 mm × 160 mm molds. The mold was covered with plastic film and situated in the curing room (20 ± 2 °C, 50 ± 5 % RH) for 24 h. Then, the specimens were removed from the mold and continued standard curing (20 ± 2 °C, 95 ± 2 % RH) to 3d and 28d.

2.3. Testing methods

2.3.1. Microscopic test

XRD, FTIR and TGA were employed to analyze the phase composition, chemical functional groups and reaction products of PHC pipe pile concrete. Before testing, paste specimens were crushed and the central part were submerged in anhydrous ethanol for 7 days to inhibit hydration. Samples were then vacuum-dried at 60 °C for 24 h, followed by pulverization to a particle size < 0.075 mm. The X-ray diffractometer (Bruker D8 Advance) was set with the scanning range of 10 ° to 70 ° and the scan speed of 1 °/min. The infrared spectrometer (Delite DH108, China) was set to a detection range of 400–4000 cm^{-1}. For TGA, the thermogravimetric analyzer (Netzsch TMA402F3, Germany) was set to a heating rate of 10 °C/min, from 30 °C to 1000 °C. SEM analysis (Zeiss Gemini 300, Germany) was conducted to examine the PHC pipe pile concrete's microstructure. To enhance the conductivity of samples, the platinum coating was applied to the surface of samples.

2.3.2. Pore structure

The pore characteristic of concrete significantly influences its performance. Therefore, concrete's pore structure was investigated by LF NMR. Its fundamental concept is to deduce the concrete's pore size distribution based on the relaxation time (T_2) of the hydrogen nuclei in water molecules within saturated concrete. The instrument used is the

Table 2
The oxide composition of SSP, GQS and OPC.

Raw materials	SiO_2	Al_2O_3	CaO	Fe_2O_3	MgO	Na_2O	K_2O	P_2O_5	MnO	LOI
SSP	14.53	5.59	31.86	34.41	4.40	0.12	0.13	0.40	4.70	3.86
GQS	84.87	6.05	1.35	2.20	0.49	0.12	0.89	0.17	0.20	3.64

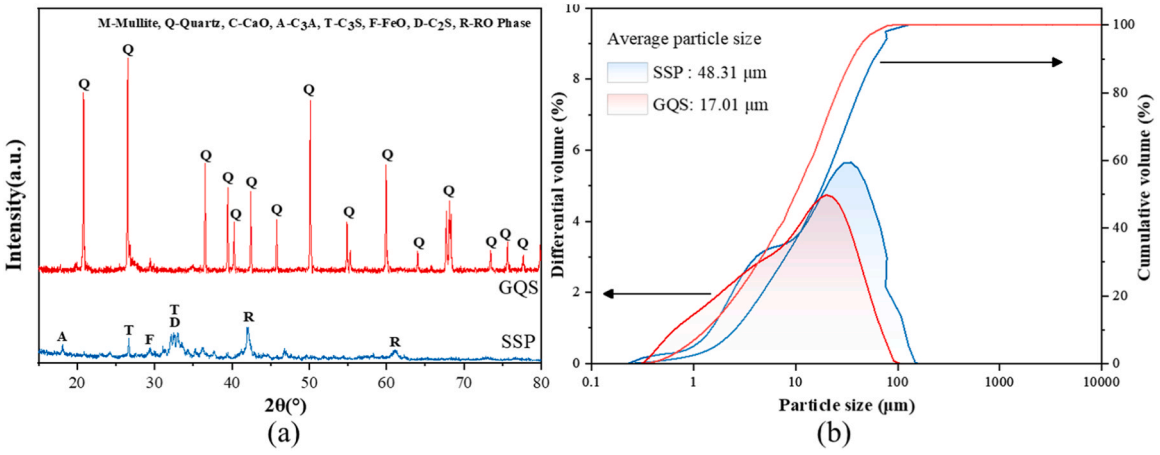

Fig. 2. (a) mineral phase composition and (b) particle size distribution of SSP and GQS.

Table 3
The test results of f-CaO and MgO contents in SSP.

Content	Measured values (%)	Standard requirement (%, GB/T 20491–2017)
f-CaO	2.7	≤ 4
MgO	4.4	≤ 5

MesoMR12–060H-1 spectrometer (Suzhou Niumag Electronic & Technology Co., Ltd., China). Before the test, the concrete specimens were diced into 50 mm cubes and subjected to 48 h vacuum water saturation. Then, the saturated sample was put into the instrument coil for relaxation test.

2.3.3. *Compressive strength test*

For mortar specimens, the compressive strength after standard curing for 28d was tested, and the activity index of each group of SCMs was calculated by formula (1). For concrete specimens, the compressive strength was evaluated after both steam curing and autoclave curing. Each group of mortar and concrete specimens tested 6 times, with results presented as averages and standard deviations.

$$AI = \frac{S_1}{S_0} \times 100 \quad \%\# \tag{1}$$

Table 5
Mix proportion of mortar specimens (unit: g).

Blended	Group code	OPC	GQS	SSP	Standard sand	Water
Mortar	M-G0S0	450	0	0	1350	225
	M-G30S0	315	135	0		
	M-G20S10	315	90	45		
	M-G10S20	315	45	90		
	M-G0S30	315	0	135		

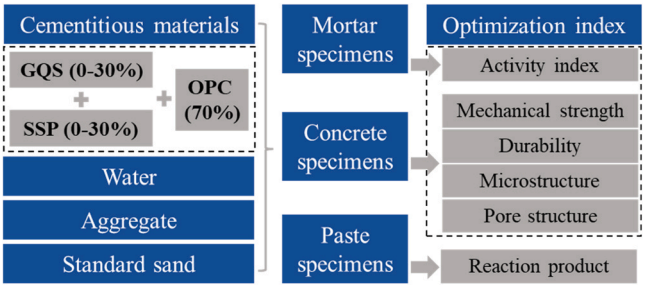

Fig. 3. The experimental research program of this study.

Table 4
Mix proportion of paste (unit: g) and concrete specimens (unit: kg/m^3).

Blended	Group code	OPC	GQS	SSP	Fine aggregate	Coarse aggregate	Water	Polycarboxylate superplasticizer
Concrete	C-G0S0	420	0	0	760	1250	118	11
	C-G30S0	294	126	0				
	C-G20S10	294	84	42				
	C-G10S20	294	42	84				
	C-G0S30	294	0	126				
Paste	P-G0S0	420	0	0			118	11
	P-G30S0	294	126	0				
	P-G20S10	294	84	42				
	P-G10S20	294	42	84				
	P-G0S30	294	0	126				

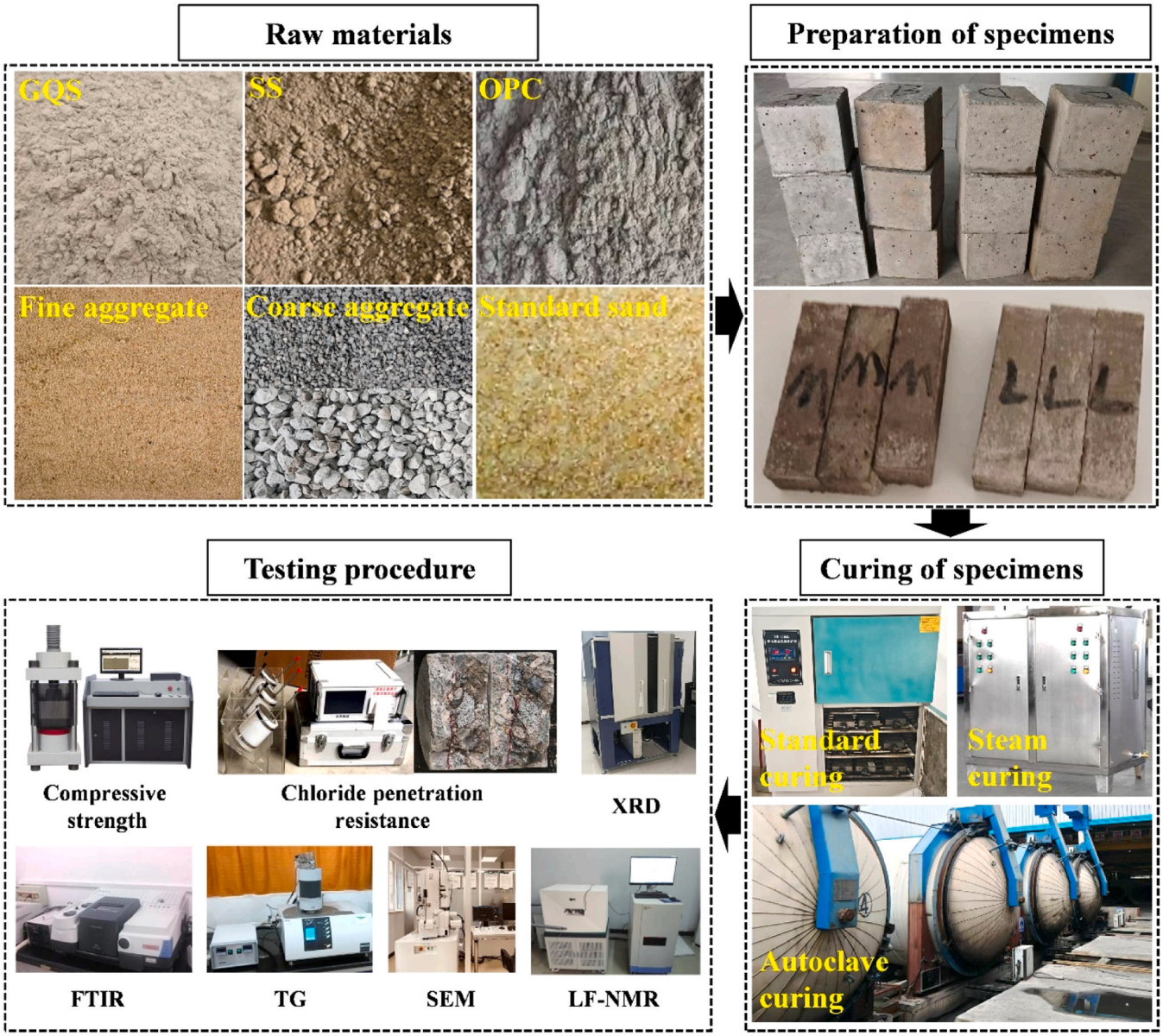

Fig. 4. The raw material preparation, mixing, curing and testing procedure in this study.

Where *AI* is the activity index, *S1* is the 28d compressive strength of mortar specimens prepared by using SCMs to replace 30 % OPC, and *S0* is the 28d compressive strength of mortar specimens prepared by using 100 % OPC.

2.3.4. Chloride penetration resistance

The Rapid Chloride Migration (RCM) test was employed to assess the resistance to chloride ion permeability of PHC pipe pile concrete. Before the test, Φ100 mm × 50 mm cylindrical specimens were prepared and followed the same curing regimes as Section 2.2. Each group of concrete specimens underwent three tests, with the mean value used as the final result.

3. Results and discussion

3.1. XRD analysis

The XRD patterns for various groups of paste specimens are shown in Fig. 6. The main mineral phases in P-G0S0 include quartz, ettringite (AFt), portlandite, calcium silicate hydrate (C-S-H) and calcite. Among them, AFt and C-S-H are produced by the hydration of C_3A, C_2S and C_3S in OPC; calcite is generated due to the carbonation of the paste during curing. After adding 30 % GQS, the intensity of the quartz diffraction peak in P-G30S0's pattern significantly increased compared to P-G0S0. This is because the main mineral phase of GQS is quartz, which has relatively low reactivity, so the addition of GQS increases the content of quartz in P-G30S0. Moreover, compared to P-G0S0, the intensity of the portlandite diffraction peak in P-G30S0's pattern decreased, and the tobermorite diffraction peak appeared. This is because the pozzolanic reaction of GQS with $Ca(OH)_2$ during autoclave curing [56], resulting in the formation of C-S-H gels. Furthermore, according to the study by A et al.[33], under autoclave curing, the quartz in GQS will react with Ca $(OH)_2$ to generate tobermorite. With the addition of SSP, because of the high content of hematite in SSP, the diffraction peak of hematite appeared in the patterns. It can be observed that portlandite diffraction peak's intensity increases as the SSP content increases. This is because, due to the higher CaO content (31.86 %) in SSP compared to GQS (1.35 %), incorporating SSP enhances the production of $Ca(OH)_2$ in paste. On the other hand, since GQS has a stronger pozzolanic effect than SSP, as the GQS content decreases, the $Ca(OH)_2$ consumed by the

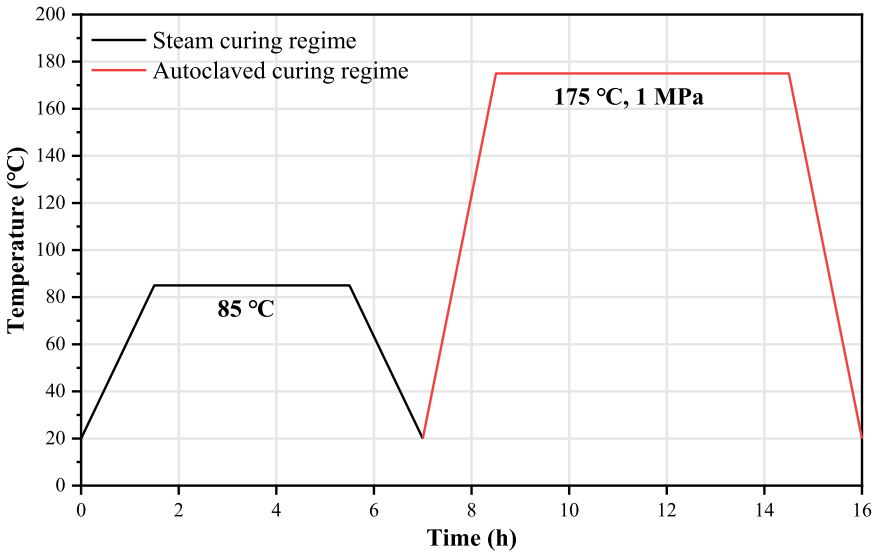

Fig. 5. Curing regimes of concrete and paste specimens.

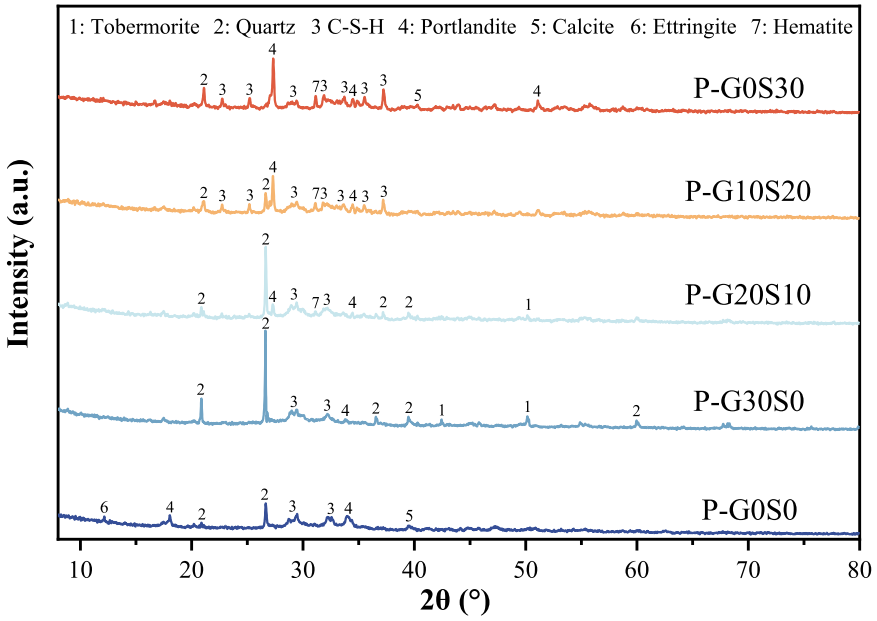

Fig. 6. XRD curves of each group of paste specimens.

pozzolanic reaction in paste also decreases. Moreover, the reduction in GQS content decreases the amount of quartz in the paste, leading to a decrease in the formation of tobermorite. Therefore, the diffraction peaks of quartz and tobermorite are weakened as the SSP content increases.

3.2. FTIR analysis

Fig. 7 displays the FTIR spectra for various groups of paste specimens. The absorption peaks at 473 cm^{-1}, 505 cm^{-1}, and 759 cm^{-1} are associated with the bending vibrations of Si-O bonds [57]. These characteristic peaks are associated with silicate minerals existing in the paste. The absorption peaks at 676 cm^{-1}, 945 cm^{-1}, and 984 cm^{-1} are attributed to the bending vibration, asymmetric stretching vibration and stretching vibration of Si-O-Si bonds [58–60]. These peaks confirm the formation of C-S-H gels. The absorption peak at 711 cm^{-1} is associated with the vibration of Al-O bonds [58], which is related to the presence of AFt in the paste. AFt is usually formed in the early stage of hydration, especially in cementitious systems containing high aluminum content. The absorption peaks at 1637 cm^{-1}, 3538 cm^{-1}, and 3644 cm^{-1} are attributed to the bending vibration and stretching vibration of O-H bonds [58,60], which typically indicate the presence of bound water in the hydration products, and further confirming the formation of gel products. The absorption peaks at 864 cm^{-1}, 1282 cm^{-1} and 1426 cm^{-1} are associated with the bending vibration, stretching vibration and stretching vibration of C-O bonds [57,60]. These peaks are related to the vibrational modes of calcite. This is because during the curing process, the carbon dioxide from the environment reacts with hydration products like portlandite, converting them into calcite.

3.3. TGA

Fig. 8 shows the TG and DTG curves for various groups of paste specimens. The TG curve's weight loss across various temperature

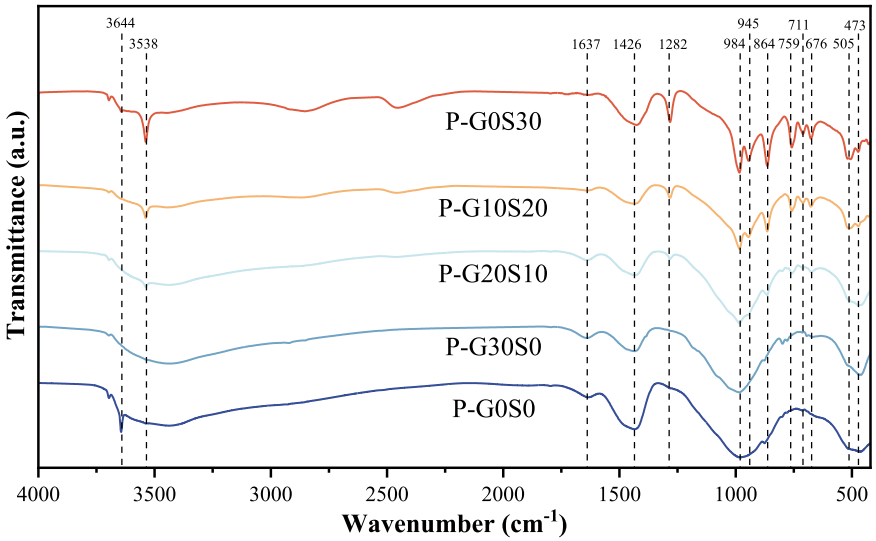

Fig. 7. FTIR spectra of each group of paste specimens.

ranges corresponds to the thermal decomposition of different reaction products. Among them, the peak in the 30–200 °C range is attributed to the dehydration process of C-S-H gels; the peak in the 400–500 °C range is associated with the decomposition of portlandite; the peak observed between 600 and 800 °C range is linked to the decomposition of calcite; the peak observed between 870 and 900 °C range is linked to tobermorite, which would convert into anhydrous wollastonite ($CaSiO_3$) at above 800 °C [61]. Notably, the TG curve of P-G0S0 exhibits a distinct broad peak in the 300–400°C range. According to the study of A et al., this is primarily caused by the dehydration of calcium aluminate hydrate (CAH) [60]. However, since the content of C_3A in GQS and SSP is significantly lower than in OPC, with the addition of SCMs, the CAH produced by C_3A hydration also diminishes, leading to a significant weakening in its endothermic peak.

As shown in Fig. 9, the relative content of reaction products can be identified based on weight loss observed across the specific temperature ranges. From Fig. 9(a), (b), and (d), it is evident that the content of C-S-H gels and tobermorite increase with the addition of GQS, while the content of portlandite decreases. This is because, as described in Section 3.1, under autoclave curing, GQS will react with $Ca(OH)_2$ to form C-S-H gels and tobermorite. However, with the addition of SSP, the $Ca(OH)_2$ consumed by GQS reduces, and SSP will generate more $Ca(OH)_2$ in paste. Consequently, the contents of C-S-H gels and tobermorite decrease with the increase of SSP, while the content of portlandite increases. As shown in Fig. 9(c), the content of calcite significantly decreases with the addition of GQS. This is because GQS not only reduces the content of CaO in the paste but also reacts to consume more $Ca(OH)_2$, thus inhibiting the carbonation reaction. As SSP content rises, the content of CaO and $Ca(OH)_2$ also increase, resulting in more calcite formed by carbonization.

3.4. Microstructure

The SEM images of concrete specimens are shown in Fig. 10. It can be observed that a large number of flocculent C-S-H gels, needle-like AFt crystals and layered $Ca(OH)_2$ crystals were produced in concrete under autoclaved curing. These hydration products can form a skeleton structure and fill the pore structure within the concrete, providing a foundation for its high strength. However, in C-G0S0, significant cracks and pores can still be observed. These cracks and pores may be related to

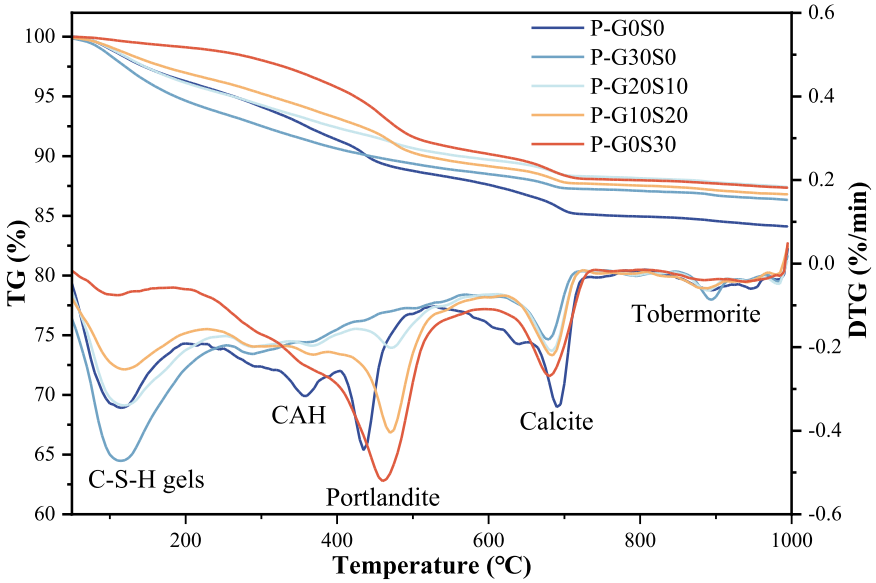

Fig. 8. TG and DTG curves of each group of pastes.

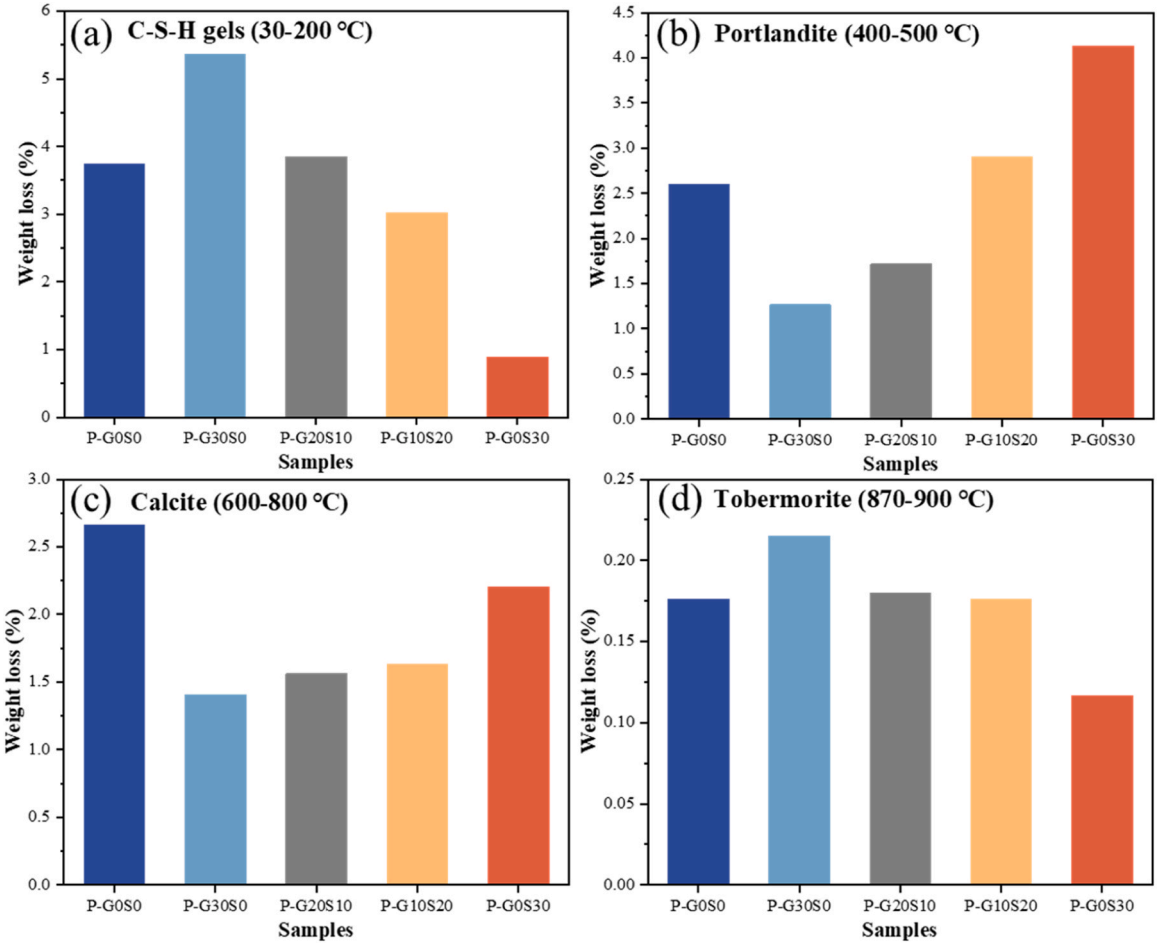

Fig. 9. Mass-normalized weight loss of each group of pastes throughout a range of temperatures: (a) 30–200 °C, (b) 400–500 °C, (c) 600–800 °C, (d) 870–900 °C.

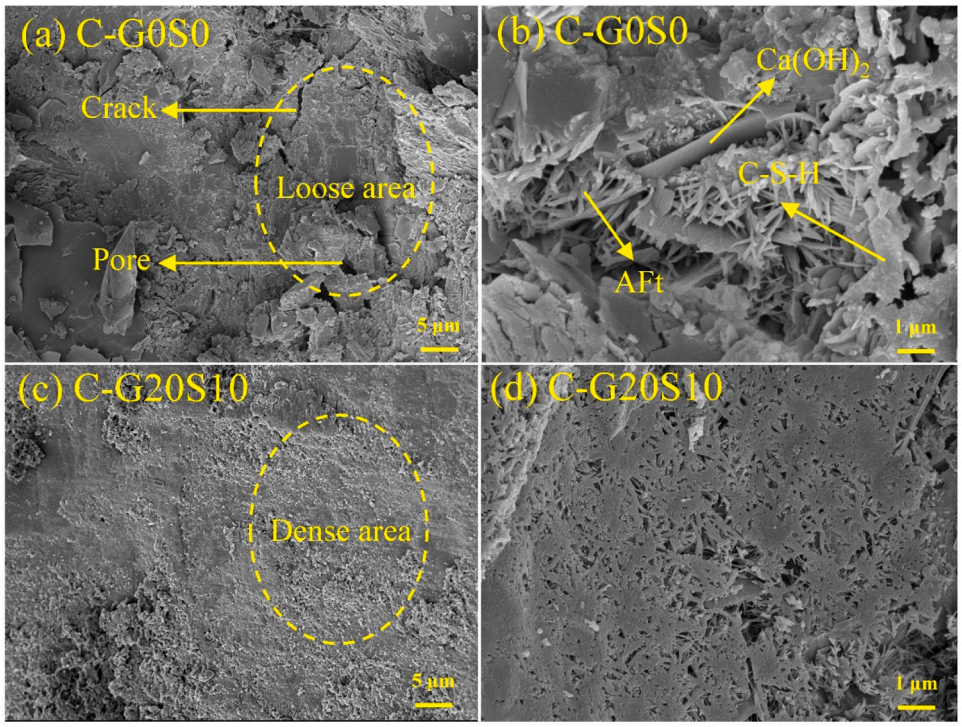

Fig. 10. SEM images of concrete specimens: (a) C-G0S0 magnified 2000 times, (b) C-G0S0 magnified 10000 times, (c) C-G20S10 magnified 2000 times, (d) C-G20S10 magnified 10000 times.

thermal stress or incomplete hydration in concrete during the curing process [3]. As shown in Fig. 10(c) and (d), with the addition of GQS and SSP, C-G20S10 exhibited a more uniform and smooth gel structure, and its microstructure showed higher compactness. This is because the addition of GQS and SSP will produce both the filling effect and the pozzolanic effect, thereby reducing the pores and improving the compactness of concrete, which will be further supported in Section 3.5.

Fig. 11 presents the interfacial transition zone (ITZ) in different group of concrete specimens. As observed in Fig. 11(a), the boundary between the aggregate and paste in C-G0S0 is relatively weak, with noticeable microcracks. This may be due to the significant difference in thermal deformation properties between the paste and aggregates, which results in inconsistent strain during the heating process. In addition, during autoclave curing, fluctuations in temperature and humidity can also produce stress differences in the concrete, further promoting the formation of strain cracks, especially in ITZ. However, as shown in Fig. 11(b) and (c), after the addition of GQS and SSP, the C-S-H gels, needle-like AFt crystal and layered $Ca(OH)_2$ crystal generated by hydration and pozzolanic reaction significantly enhanced the compactness of ITZ, thereby enhancing the adhesion between the paste and the aggregate and hindering the generation of microcracks in the ITZ. When the SSP content increases to 30 %, as shown in Fig. 11(d), microcracks appear again in C-G0S30's ITZ. This could be linked to the reduced hydration products in C-G0S30. As described in TGA results. The reduction in hydration products leads to insufficient bonding strength between the paste and aggregates, resulting in cracks developing in the ITZ, subsequently affecting the overall strength of the concrete.

3.5. Pore structure

The pore structure of different groups of concrete specimens is shown in Fig. 12. According to previous studies [62–64], the pores in concrete can be classified based on their pore size. Gel pore (1–10 nm) is formed by hydration products (especially C-S-H gels); transition pore (10–100 nm) is primarily formed by gases released during the hydration reaction; capillary pore (100–1000 nm) primarily results from the unreacted free water in the concrete; macropore (>1000 nm) is typically large pores formed by underfilled aggregate-paste interface defects, cracks, or external factors such as air bubbles. As illustrated in Fig. 12 (a), the concrete's total porosity gradually decreases with the addition of SCMs. The total porosity for C-G0S0, C-G30S0, C-G20S10, C-G10S20, and C-G0S30 are 6.83 %, 6.71 %, 5.51 %, 5.47 %, and 5.07 %, respectively. The decrease in total porosity results from the filling and pozzolanic effect of SCMs, showing that incorporating GQS and SSP can optimize concrete's pore structure. Notably, the content of gel pore in concrete reaches the highest with the addition of 30 % GQS, and then decreases with the increase of SSP in SCMs. This trend aligns with the variation of C-S-H gel content illustrated in Fig. 9(a), further proving that the pozzolanic effect of GQS under autoclave curing is greater than that of SSP. As illustrated in Fig. 12(b), the concrete's pore distribution curve shows three primary peaks. The first peak relates to pore sizes between 1 and 100 nm, representing gel pore and transition pore; the second peak corresponds to pore sizes of 100–1000 nm, representing capillary pore; and the third peak is associated with pore sizes greater than 1000 nm, representing macropore. It can be observed that the area of the first peak in each group of concrete specimens is greater than 70 %, indicating that gel pore and transition pore account for the vast majority of concrete's pores. Moreover, after the addition of SCMs, it can be observed that, compared to C-G0S0, the first peak in the curves for the other four groups shifts towards smaller pore sizes, demonstrating that incorporating GQS and SSP refines the concrete's pore structure.

3.6. RCM results

The results of RCM test for each group of concrete specimens are displayed in Fig. 13. It can be seen that the chloride ion diffusion coefficient of concrete was significantly influenced by the incorporation of SCMs. The control group C-G0S0 exhibited a diffusion coefficient of 5.31×10^{-12} m^2/s, whereas the incorporation of 30 % GQS in C-G30S0 reduced this value to 2.38×10^{-12} m^2/s (a 44.8 % decrease). This is attributed to the dual mechanism of GQS's filling effect and pozzolanic reaction, which synergistically refines the pore structure and inhibits chloride ion penetration. When progressively replacing GQS with SSP,

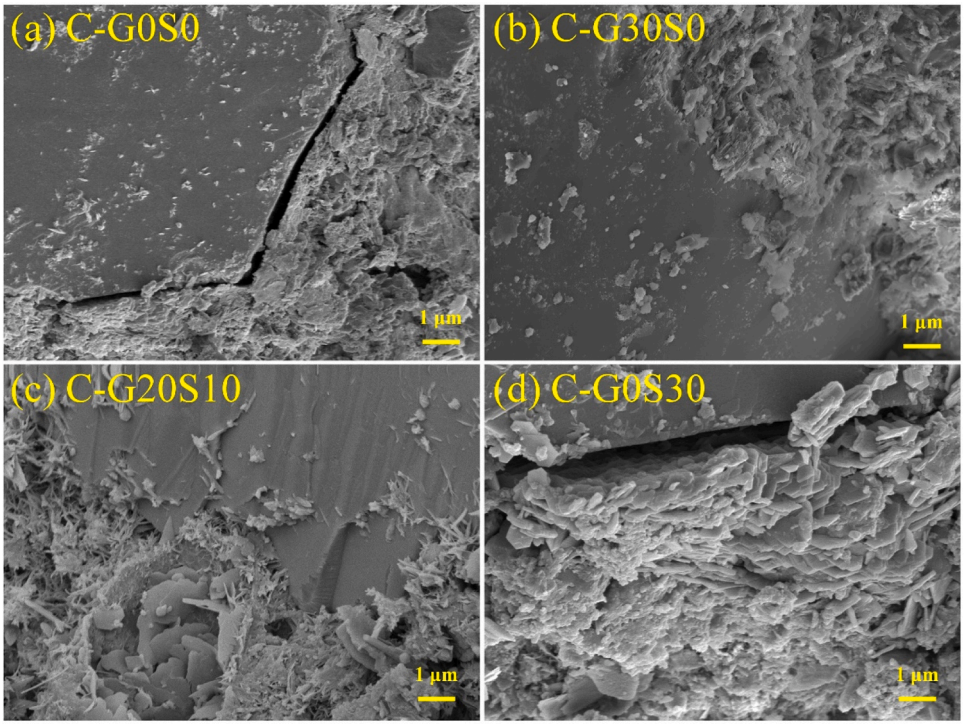

Fig. 11. The ITZ between paste and aggregates in concrete specimens: (a) C-G0S0, (b) C-G30S0, (c) C-G20S10, (d) C-G0S30.

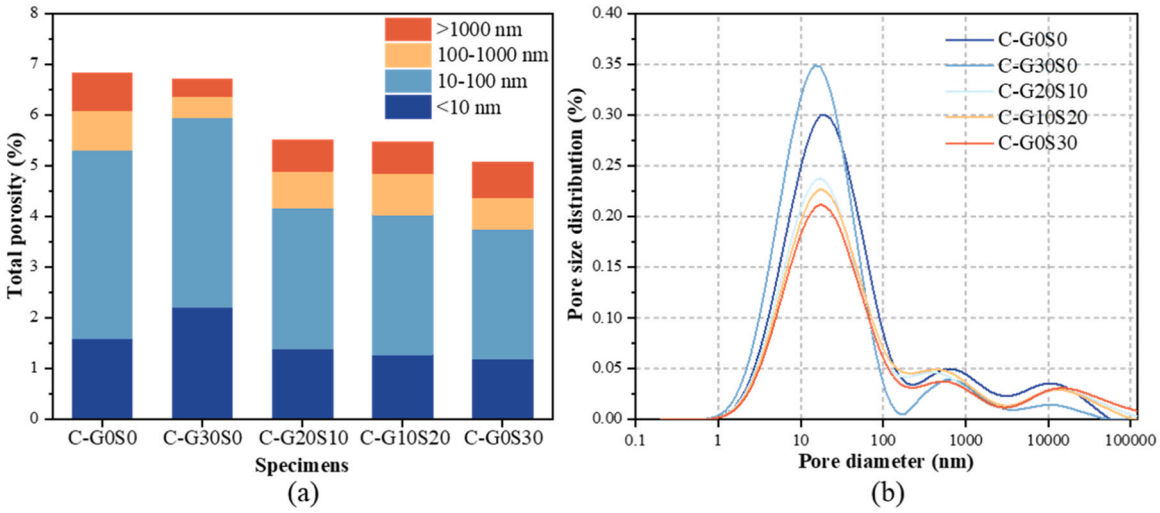

Fig. 12. Pore structure of different groups of concrete specimens: (a) total porosity and proportion of different sizes of pores, (b) pore size distribution.

the chloride ion diffusion coefficients of C-G20S10, C-G10S20, and C-G0S30 were 2.81 × 10^{-12} m^2/s, 3.12 × 10^{-12} m^2/s, and 3.01 × 10^{-12} m^2/s, respectively, indicating a parabolic trend: initially increasing by 18.1 % and 31.1 % with SSP substitution, then decreasing by 3.5 % at full SSP replacement. Notably, the chloride ion diffusion coefficient of all concrete specimens prepared using SCMs was significantly lower than that of the control group C-G0S0, suggesting that the incorporation of both GQS and SSP can enhance the resistance of concrete to chloride ion penetration. According to the research of Li et al. [56], the concrete's pores can be divided into harmless pores (<50 nm) and harmful pores (>50 nm). Compared with harmless pores with smaller pore size, harmful pores, with larger pore sizes, negatively impact the concrete's permeability and strength. Therefore, the porosity of harmful and harmless pores in different groups of concrete specimens was calculated based on the LF NMR results presented in Section 3.5, as shown in Fig. 14.

As shown in Fig. 13 and Fig. 14, the variation trend of harmful pore's porosity in concrete is generally consistent with the trend of their chloride ion diffusion coefficients. Specifically, after adding 30 % GQS, although the total porosity of C-G30S0 is only slightly lower than that of C-G0S0, the porosity of harmful pore in C-G30S0 (1.24 %) decreased by 55.6 % compared to C-G0S0 (2.23 %). This suggests that incorporating GQS effectively improved the pore structure by reducing large pores, thereby significantly decreasing the diffusion path for chloride ions. As SSP content in SCMs rises, although the total porosity of C-G20S10 and C-G10S20 decreased, their porosity of harmful pore was significantly higher than C-G30S0, resulting in increased chloride ion diffusion coefficient. As described in Section 3.4, the increase in harmful pores may be attributed to the reduction in gel products, which leads to strain cracks in the ITZ of the concrete under steam curing. However, the chloride ion diffusion coefficients of C-G20S10 and C-G10S20 were still significantly lower than C-G0S0, indicating the incorporating of GQS and SSP can effectively enhance the concrete's resistance to chloride ion permeability. When the SSP content reached 30 %, C-G0S30 exhibited diminished total porosity and harmful pore's porosity, resulting in the decrease of its chloride ion diffusion coefficient again.

3.7. Compressive strength

Fig. 15 displays the compressive strength and activity index of various group of mortar specimens. Compared with the control group M-G0S0, the incorporation of GQS notably reduced the mortar's

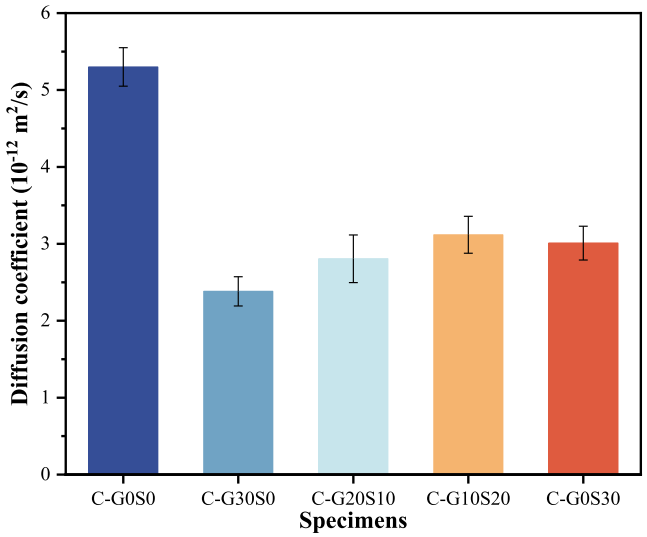

Fig. 13. Chloride diffusion coefficient of different groups of concrete specimens.

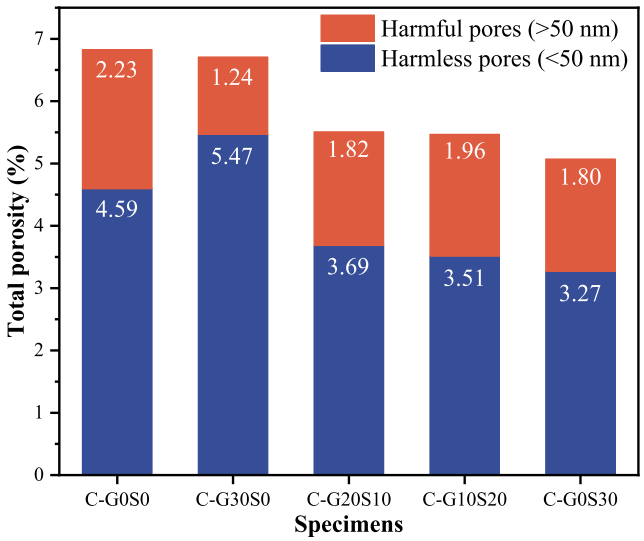

Fig. 14. The porosity of harmful pores and harmless pores in different groups of concrete specimens.

compressive strength, with the activity index of M-G30S0 being only 64.9 %, which further proves that the cementitious activity of GQS is low. As the increase of SSP, the mortar's compressive strength gradually improved, and the activity index of M-G0S30 reached 80.8 %, but it was still lower than M-G0S0. The main mineral phase in GQS is quartz, which has low hydration activity under standard curing conditions, and hard to directly participate in hydration reactions to generate gel products. With the addition of SSP, because it contains a certain amount of active mineral phases such as C_2S and C_3S, which can hydrate to form gel products, so it can enhance the mortar's strength. However, SSP still contains a significant amount of low-activity crystalline phases. Therefore, despite the rise in SSP content, the enhancement in mortar's strength remains limited.

Fig. 16 illustrates the compressive strength of various group of concrete specimens after steam and autoclave curing. In industrial production, before autoclave curing, PHC pipe piles must first undergo steam curing in molds to ensure sufficient demolding strength. Due to the large volume of PHC pipe piles, if the strength is insufficient during demolding, it is prone to cracking and deformation. Therefore, PHC pipe pile concrete should typically achieve a minimum compressive strength of 45 MPa after steam curing. It can be observed from Fig. 16(a) that after steam curing, the compressive strength of concrete specimens follows a similar trend as shown in Fig. 15(a), with all exceeding 45 MPa, which meets the requirements of demolding. Notably, the compressive strengths of C-G30S0, C-G20S10, C-G10S20, and C-G0S30 (45.3 MPa, 46.4 MPa, 47.5 MPa, and 48.7 MPa, respectively) reached 87.9 %, 90.1 %, 92.2 %, and 94.6 % of the control group C-G0S0 (51.5 MPa), which is greatly higher than the activity index, showing that the cementitious activity of GQS and SSP under steam curing is notably improved. As shown in Fig. 16(b), the compressive strength of concrete specimens after autoclaved curing increases first and then decreases, and all exceed 80 MPa. Among them, the compressive strength of C-G30S0 and C-G20S10 (96.1 MPa and 97.5 MPa) is even higher than that of the control group C-G0S0 (94.3 MPa). This is because as mentioned earlier, under autoclave curing conditions, the filling effect and pozzolanic effect of GQS and SSP reduced the concrete's porosity and optimized the concrete's pore structure, thus improving its compressive strength. However, with SSP content rising to 20 % or higher, the reduction in hydration products and the rise in harmful pore content led to a lower compressive strength of the concrete. Considering both the demolding strength and the compressive strength after autoclave curing of PHC pipe pile concrete, the optimal mix ratio of composite SCMs is 20 % GQS and 10 % SSP.

4. Conclusions

In this study, GQS and SSP were used as composite SCMs to replace 30 % of OPC to prepare PHC pipe pile concrete, and the effects of GQS and SSP on the reaction products, microstructure, pore structure, mechanical properties and durability of PHC pipe pile concrete were studied. The main findings of this study are as follows:

(1) Under autoclave curing, GQS not only undergoes pozzolanic reactions to generate C-S-H gels but also reacts with $Ca(OH)_2$ to form tobermorite. However, when the SSP content in SCMs increases, due to its weaker pozzolanic effect compared to GQS and higher CaO content, the content of C-S-H gels in paste decreases, and the content of $Ca(OH)_2$ increases.
(2) The use of GQS and SSP as composite SCMs not only improves the microstructure of the ITZ between paste and aggregates in PHC pipe pile concrete, but also reduces the porosity of concrete and improves its pore structure, thereby increasing the compactness of concrete and enhancing its resistance to chloride ion permeability.
(3) The cementitious activity of SSP is significantly higher than that of GQS, so the compressive strength of PHC pipe pile concrete under steam curing increases with the increase of SSP, which is beneficial to avoid cracking of concrete due to insufficient strength during demolding. Under autoclaved curing, due to the enhanced pozzolanic effect and improved pore structure, the compressive strength of PHC pipe pile concrete prepared by composite SCMs reached a maximum of 97.5 MPa after autoclave curing.
(4) When the GQS content is 20 % and the SSP content is 10 %, the composite SCMs achieve the greatest overall improvement in the pore structure, durability and mechanical strength of PHC pipe pile concrete. Specifically, compared to the control group with 100 % OPC, the concrete's porosity decreased by 19.3 %, the chloride ion diffusion coefficient decreased by 47.1 % and the compressive strength increased by 3.4 %. This indicate that the use of GQS and SSP as composite SCMs for the production of PHC pipe pile concrete has broad application prospects.

5. Recommendations

The findings of this study provide valuable insights into the potential of using SSP and GQS as composite SCMs for the preparation of PHC pipe piles. However, additional large-scale trials and field tests are required

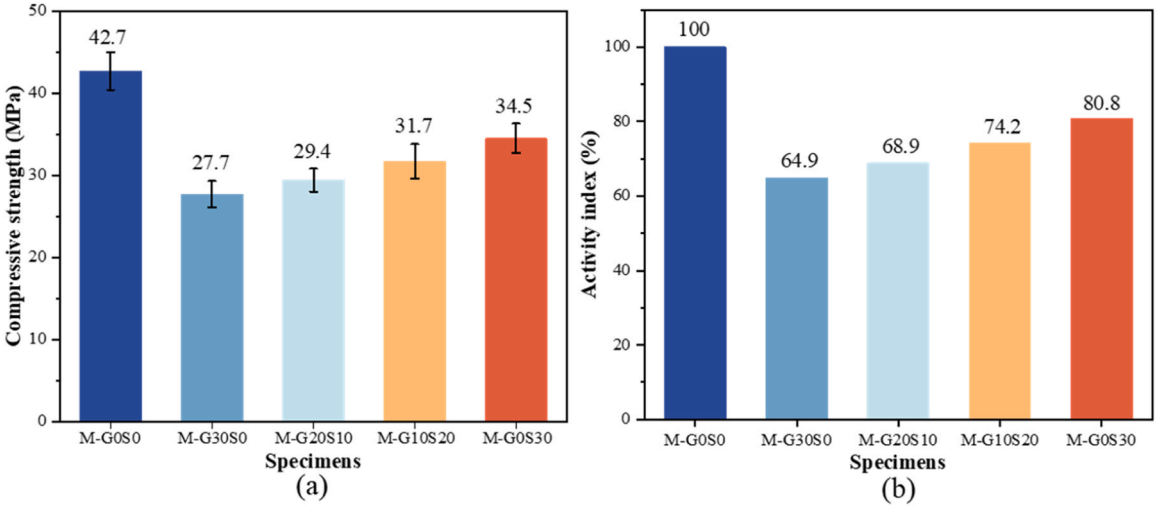

Fig. 15. The 28d compressive strength and activity index of different groups of mortar specimens, (a) 28d compressive strength, (b) activity index.

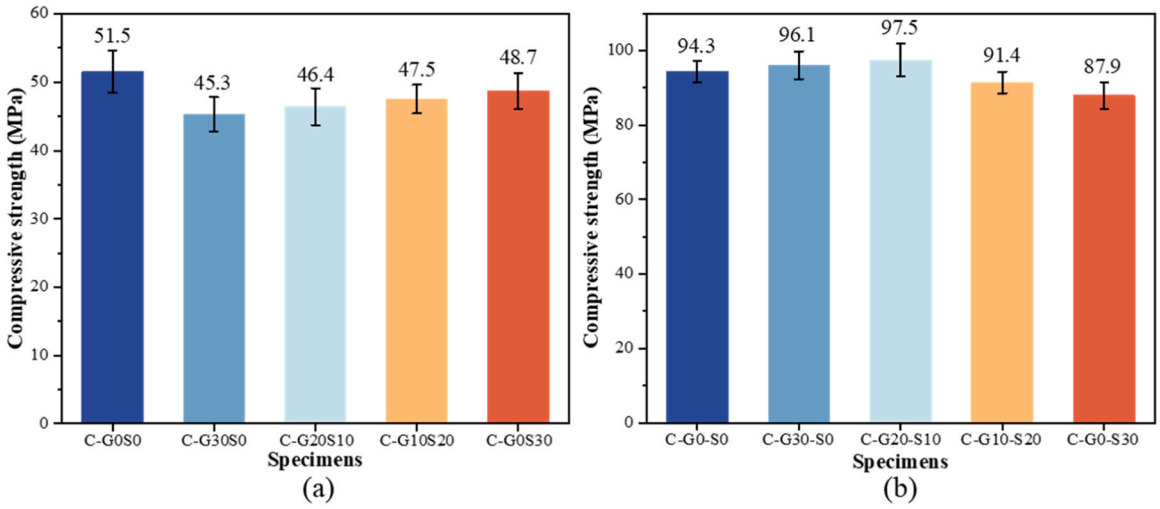

Fig. 16. The compressive strength of concrete specimens after steam curing and autoclaved curing, (a) steam curing, (b) autoclaved curing.

to confirm the practical feasibility and long-term performance of PHC pipe piles made with this novel composite SCMs. In addition, the effects of GQS and SSP need to be compared with other commonly used SCMs (such as fly ash or slag powder) to obtain a more comprehensive understanding of the comparative advantages and performance of different SCMs in PHC pipe pile applications.

Another critical aspect that warrants further attention is the leaching behavior of heavy metals from SSP when used in concrete applications, especially when applied for foundation reinforcement. Given the relatively high content of heavy metals in steel slag, it is essential to assess the potential environmental risks associated with the leaching of toxic ions such as lead, cadmium, and chromium, which may occur over time under certain conditions.

In summary, future research will focus on validating the effect of composite SCMs on the performance of PHC pipe piles in engineering application, and compare it with other commonly used SCMs. In addition, the leaching behavior of heavy metal ions from PHC pipe piles will be also evaluated to ensure environmental safety during long-term use.

CRediT authorship contribution statement

Xinkui Yang: Conceptualization, Methodology, Writing – Original Draft. **Botao Tu:** Conceptualization, Methodology. **Shaopeng Wu:** Conceptualization, Methodology. **Shi Xu:** Investigation, Formal analysis. **Yu Song:** Supervision, Writing - review & editing. **Dongyu Chen:** Methodology, Supervision, Writing - review & editing. **Chao Yang:** Investigation, Formal analysis.

Declaration of Competing Interest

The authors declare that they have no known competing financial interests or personal relationships that could have appeared to influence the work reported in this paper.

Acknowledgments

This work was supported by the National Natural Science Foundation of China (No. 52378461, No. 52208444 and No. 52068061), the project of Hebei Provincial Department of Transportation (No. 202319), the Science and Technology Project of the Department of Transportation of Guangxi Autonomous Region (No. 2021-MS5–125), the Hubei Science and Technology Innovation Talent and Service Project (No. 2022EHB006) and State Key Laboratory of Silicate Materials for Architectures (Wuhan University of Technology) (SYSJJ2024–06).

Data availability

Data will be made available on request.

References

[1] Z. Yang, G. Li, W. Wang, Y. Lv, Study on the Flexural Performance of Prestressed High Strength Concrete Pile, KSCE J. Civ. Eng. 22 (10) (2018) 4073–4082.
[2] W. Shao, J. Li, Service life prediction of cracked RC pipe piles exposed to marine environments, Constr. Build. Mater. 64 (2014) 301–307.
[3] F. Liu, W. Feng, Z. Xiong, L. Li, Y. Yang, H. Lin, Y. Shen, Impact performance of new prestressed high-performance concrete pipe piles manufactured with an environmentally friendly technique, J. Clean. Prod. 231 (2019) 683–697.
[4] X. Han, Z. Du, P. Wang, R. Zhang, J. Gao, Z. Ling, D. Wei, Multi-scale microstructure quantitative characterization and anti-erosion performance of PHC pipe pile, Constr. Build. Mater. 406 (2023) 133464.
[5] Z. Zhang, J. Wei, X. Xing, F. Ma, B. Wang, N. Xu, M. Li, J. Geng, L. Chen, W. Zhu, Q. Yu, Studying the interfacial transition zone microstructure of pre-stressed high-strength concrete pipe piles, Constr. Build. Mater. 448 (2024) 138045.
[6] P. Zhou, K. Gu, Z. Jiang, Preparation and properties of non-autoclaved high-strength pile concrete with anhydrite and ground granulated blast-furnace slag, Case Stud. Constr. Mater. 21 (2024) e03597.
[7] J. Han, Z. Shui, G. Wang, T. Sun, X. Gao, Performance evaluation of steam cured HPC pipe piles produced with metakaolin based mineral additives, Constr. Build. Mater. 189 (2018) 719–727.
[8] J. Yang, J. Zeng, X. He, Y. Zhang, Y. Su, H. Tan, Sustainable clinker-free solid waste binder produced from wet-ground granulated blast-furnace slag, phosphogypsum and carbide slag, Constr. Build. Mater. 330 (2022) 127218.
[9] Z. Wang, Z. Shui, T. Sun, X. Li, M. Zhang, Recycling utilization of phosphogypsum in eco excess-sulphate cement: Synergistic effects of metakaolin and slag additives on hydration, strength and microstructure, J. Clean. Prod. 358 (2022) 131901.
[10] W. Liu, J. Wang, S. Wu, Q. Liu, H. Xu, Analysis of the influence of interface features on shear strength between thin overlay and base layer via random forest regression, Constr. Build. Mater. 462 (2025) 139870.
[11] P. Cui, S. Wu, Y. Xiao, R. Hu, T. Yang, Environmental performance and functional analysis of chip seals with recycled basic oxygen furnace slag as aggregate, J. Hazard. Mater. 405 (2021) 124441.
[12] H. Xu, Y. Zou, G. Airey, H. Wang, H. Zhang, S. Wu, A. Chen, Wetting of bio-rejuvenator nanodroplets on bitumen: A molecular dynamics investigation, J. Clean. Prod. 444 (2024) 141140.
[13] C. Yang, S. Wu, J. Xie, S. Amirkhanian, Z. Zhao, H. Xu, F. Wang, L. Zhang, Development of blending model for RAP and virgin asphalt in recycled asphalt mixtures via a micron-Fe3O4 tracer, J. Clean. Prod. 383 (2023).
[14] W. Wang, X. Cai, W. Zhou, Y. Wang, Mechanical properties and statistical analysis of Engineered Cementitious Composites (ECC) with ultrahigh-volume limestone powder incorporating several supplementary cementitious materials, Constr. Build. Mater. 457 (2024) 139432.
[15] P.R. Cunningham, L. Wang, S. Nassiri, P. Thy, J.T. Harvey, B.M. Jenkins, S. A. Miller, Compressive strength and regional supply implications of rice straw and rice hull ashes used as supplementary cementitious materials, Resour., Conserv. Recycl. 214 (2025) 108024.
[16] S. Qing, C. Li, Mechanical properties and microstructure of low carbon high-strength engineered cementitious composites with supplementary cementitious material, Case Stud. Constr. Mater. 22 (2025) e04164.
[17] M. Zajac, R. Bremeier, J. Deja, M. Król, M. Ben Haha, Carbonation hardening of Portland cement with recycled supplementary cementitious materials, Cem. Concr. Compos. 157 (2025) 105904.

[18] L. Campagiorni, M. Tonelli, F. Ridi, Synergistic effect of limestone and supplementary cementitious materials in ternary blended cements, Curr. Opin. Colloid Interface Sci. 75 (2025) 101885.
[19] G. Carneiro, T. Bier, S. Waida, A. Dous, S. Heinemann, P. Herr, A. Charitos, Treatment of Energy from Waste Plant fly-ash for blast furnace slag substitution as a Supplementary Cementitious Material, J. Clean. Prod. 490 (2025) 144693.
[20] X. Ma, H. Hu, Y. Luo, W. Yao, Y. Wei, A. She, A carbon footprint assessment for usage of recycled aggregate and supplementary cementitious materials for sustainable concrete: A life-cycle perspective in China, J. Clean. Prod. 490 (2025) 144772.
[21] A. Hazarika, L. Huang, S. Erlingsson, K. de Weerdt, I. Löfgren, S. Iftikhar, A. Babaahmadi, Characterization, activation and reactivity – A case study of Nordic volcanic materials for application as Supplementary Cementitious Materials, Case Stud. Constr. Mater. 22 (2025) e04096.
[22] L. Jia, E. Dong, Z. Jia, Y. Jiang, Z. Tang, K. Xia, Y. Gao, Y. Zhang, Influence of different supplementary cementitious materials on water distribution and rheological behavior of blended cement paste, Constr. Build. Mater. 443 (2024) 137705.
[23] X. Shang, B. Gong, J. Chang, Y. Chen, J. Yang, G. Ou, Y. Wang, Turning corn straw waste into supplementary cementitious materials: Feasibility, properties and life cycle assessment, Constr. Build. Mater. 455 (2024) 139177.
[24] Z. Liu, K. Takasu, H. Koyamada, H. Suyama, A study on engineering properties and environmental impact of sustainable concrete with fly ash or GGBS, Constr. Build. Mater. 316 (2022) 125776.
[25] D. Shen, K. Liu, C. Wen, Y. Shen, G. Jiang, Early-age cracking resistance of ground granulated blast furnace slag concrete, Constr. Build. Mater. 222 (2019) 278–287.
[26] E.D. Adesanya, A.T.M. Marsh, S. Krishnan, J. Yliniemi, S.A. Bernal, Co-calcination of kaolinitic clay and green liquor dregs to produce supplementary cementitious materials, Case Stud. Constr. Mater. 22 (2025) e04520.
[27] B. Yang, X. Gu, Z. Li, B. Liu, Y. Wang, Q. Wang, J. Liu, Synergistic effects of lithium slag and coarse limestone powder as supplementary cementitious materials: Hydration and microstructure, J. Build. Eng. 99 (2025) 111608.
[28] N. Bheel, I.M. Chohan, A.A. Ghoto, S.A. Abbasi, E.M. Tag-eldin, H.R. Almujibah, M. Ahmad, O. Benjeddou, R.A. Gonzalez-Lezcano, Synergistic effect of recycling waste coconut shell ash, metakaolin, and calcined clay as supplementary cementitious material on hardened properties and embodied carbon of high strength concrete, Case Stud. Constr. Mater. 20 (2024) e02980.
[29] J.-C. Liu, M.U. Hossain, D. Xuan, H.A. Ali, S.T. Ng, H. Ye, Mechanical and durability performance of sustainable concretes containing conventional and emerging supplementary cementitious materials, Dev. Built Environ. 15 (2023) 100197.
[30] G. Li, J. Zhou, J. Yue, X. Gao, K. Wang, Effects of nano-SiO2 and secondary water curing on the carbonation and chloride resistance of autoclaved concrete, Constr. Build. Mater. 235 (2020) 117465.
[31] P. Wang, H. Fu, W. Zuo, S. Luo, H. Zhao, P. Feng, H. Wang, Effect of n-C-S-H-PCE and slag powder on the autogenous shrinkage of high-strength steam-free pipe pile concrete, Constr. Build. Mater. 325 (2022) 126815.
[32] L.L. Xue, Y. Shen, Effect of Mineral Admixture on Mechanical Property of PHC Pile Concrete, Adv. Mater. Res. 919-921 (2014) 1775–1779.
[33] Q. Yang, S. Zhang, S. Huang, Y. He, Effect of ground quartz sand on properties of high-strength concrete in the steam-autoclaved curing, Cem. Concr. Res. 30 (12) (2000) 1993–1998.
[34] X. Han, D. Wei, P. Wang, M. Wang, Z. Du, Z. Ling, Microstructure characteristics and evolution of pipe pile concrete under centrifugation and steam curing, Constr. Build. Mater. 450 (2024) 138554.
[35] Y. Hu, L. Ma, T. He, Effect of Mineral Admixtures on the Sulfate Resistance of High-Strength Piles Mortar, Materials 13 (16) (2020) 3500.
[36] W. Li, M. Cao, F. Liu, D. Wang, J. Chang, Pretreatment of alkali activation and carbonation of steel slag for using as binding material, Cem. Concr. Compos. 149 (2024) 105521.
[37] X. Zhu, H. Hou, X. Huang, M. Zhou, W. Wang, Enhance hydration properties of steel slag using grinding aids by mechanochemical effect, Constr. Build. Mater. 29 (2012) 476–481.
[38] N. Yong-Sing, L. Yun-Ming, H. Cheng-Yong, M.M.A.B. Abdullah, P. Pakawanit, L. W.L. Chan, N. Hui-Teng, O. Shee-Ween, O. Wan-En, H. Yong-Jie, Thin fly ash/ ladle furnace slag geopolymer: Effect of elevated temperature exposure on flexural properties and morphological characteristics, Ceram. Int. 48 (12) (2022) 16562–16575.
[39] Y. Song, H. Xu, S. Wu, J. Xie, A. Chen, Y. Lv, Y. Cheng, Y. Li, High-quality utilization of reclaimed asphalt pavement (RAP) in asphalt mixture with the enhancement of steel slag and epoxy asphalt, Constr. Build. Mater. 445 (2024) 137963.
[40] C. Yang, S. Wu, P. Cui, S. Amirkhanian, Z. Zhao, F. Wang, L. Zhang, M. Wei, X. Zhou, J. Xie, Performance characterization and enhancement mechanism of recycled asphalt mixtures involving high RAP content and steel slag, J. Clean. Prod. 336 (2022) 130484.
[41] L. Li, X. Wu, C. Wang, T.-C. Ling, Carbonated steel slag as supplementary cementitious material: Paving the way to full reutilization, Case Stud. Constr. Mater. 22 (2025) e04535.
[42] J. Gu, C. Wei, P. Wu, Z. Cao, Y. Shao, X. Liu, Z. Zhang, Application and mechanism analysis of steel slag in resource recovery and environmental remediation: A review, Miner. Eng. 227 (2025) 109268.
[43] S.S. Chandel, A. Lavakumar, N.S. Randhawa, P.K. Singh, Unique hot stage modification technique to enhance cementitious properties of electric arc furnace steel slag, J. Environ. Manag. 376 (2025) 124398.
[44] J. Li, Q. Hou, X. Zhang, X. Zhang, Microbial-induced mineral carbonation: A promising approach for improving Carbon sequestration and performance of steel slag for its engineering utilization, Dev. Built Environ. 21 (2025) 100615.
[45] J. Zhao, Z. Li, D. Wang, P. Yan, L. Luo, H. Zhang, H. Zhang, X. Gu, Hydration superposition effect and mechanism of steel slag powder and granulated blast furnace slag powder, Constr. Build. Mater. 366 (2023) 130101.
[46] S. Zhuang, Q. Wang, Inhibition mechanisms of steel slag on the early-age hydration of cement, Cem. Concr. Res. 140 (2021) 106283.
[47] Y. Zhao, P. Wu, J. Qiu, Z. Guo, Y. Tian, X. Sun, X. Gu, Recycling hazardous steel slag after thermal treatment to produce a binder for cemented paste backfill, Powder Technol. 395 (2022) 652–662.
[48] Z. Zhang, P. Cao, Y. Wang, X. Zhao, J. Liu, Effect of Fe and Mn on the hydration activity of f-CaO in steel slag, Constr. Build. Mater. 421 (2024) 135719.
[49] X. Ji, J. Hou, Y. Liu, J. Liu, Effect of CaO-FeO-MnO system solid solution on the hydration activity of tri-component f-CaO in steel slag, Constr. Build. Mater. 225 (2019) 476–484.
[50] S. Zhuang, Q. Wang, T. Luo, Modification of ultrafine blast furnace slag with steel slag as a novel high-quality mineral admixture to prepare high-strength concrete, J. Build. Eng. 71 (2023) 106501.
[51] T. Luo, X. Wang, S. Zhuang, Value-added utilization of steel slag as a hydration heat controlling material to prepare sustainable and green mass concrete, Case Stud. Constr. Mater. 19 (2023) e02619.
[52] M. Li, X. Liang, L. Chen, S. Liu, Hydration properties of composite cementitious materials containing steel slag under steam curing condition, Adv. Cem. Res. 36 (8) (2023) 394–405.
[53] Steel slag powder used for cement and concrete: GB/T 20491-2017, Technical Committee on Steel of Standardization Committee of China, 2017.
[54] Method for the determination of free calcium oxide in steel slag: YB/T 4328-2012, Technical Committee on Steel of Standardization Committee of China, 2012.
[55] Technical code for application of mineral admixture: GB/T 51003-2014, China Academy of Building Research, 2014.
[56] G. Li, X. Chen, Y. Zhang, Z. Zhuang, Y. Lv, Studies of nano-SiO2 and subsequent water curing on enhancing the frost resistance of autoclaved PHC pipe pile concrete, J. Build. Eng. 69 (2023) 106209.
[57] R. Sun, P. Shen, D. Wang, J. Wang, Z. Liu, K. Fang, Enhancing hydration of steel slag-based composite cementitious material: Synergistic effect of triisopropanolamine (TIPA) and sulfite/sulfate, Cem. Concr. Res. 184 (2024) 107619.
[58] X. Yang, S. Wu, S. Xu, B. Chen, D. Chen, F. Wang, J. Jiang, L. Fan, L. Tu, Effects of GBFS content and curing methods on the working performance and microstructure of ternary geopolymers based on high-content steel slag, Constr. Build. Mater. 410 (2024) 134128.
[59] C. Liu, Z. Li, S. Nie, J. Skibsted, G. Ye, Structural evolution of calcium sodium aluminosilicate hydrate (C-(N-)A-S-H) gels induced by water exposure: The impact of Na leaching, Cem. Concr. Res. 178 (2024) 107432.
[60] Y. Zhang, G. Zhu, Y. Zhang, X. Wu, F. Zhang, J. Zhang, X. Li, Hydration behavior and cementitious properties of steel slag: From an early age to a long-term, Case Stud. Constr. Mater. 20 (2024) e03066.
[61] S. Luo, Z. Jiang, M. Zhao, L. Yang, J. Castro-Gomes, S. Wei, T. Mi, Microwave hydrothermal synthesis of tobermorite for the solidification of iron, Case Stud. Constr. Mater. 19 (2023) e02267.
[62] S. Bhattacharja, M. Moukwa, F. D"Orazio, J.Y. Jehng, W.P. Halperin, Microstructure determination of cement pastes by NMR and conventional techniques, Adv. Cem. Based Mater. 1 (2) (2016) 67–76.
[63] D. Hou, T. Zhao, H. Ma, Z. Li, Reactive Molecular Simulation on Water Confined in the Nanopores of the Calcium Silicate Hydrate Gel: Structure, Reactivity, and Mechanical Properties, J. Phys. Chem. C. 119 (3) (2015) 1346–1358.
[64] Q. Zhang, G. Ye, E. Koenders, Investigation of the structure of heated Portland cement paste by using various techniques, Constr. Build. Mater. 38 (2013) 1040–1050.